Received 2 September 2024; Accepted 11 November 2024
https://doi.org/10.48612/letters/2024-4-419-424
https://elibrary.ru/yemwjl

Competition between the formation and decomposition of a solid solution in Al-Mg alloys during high-pressure torsion

B. B. Straumal†[1], O. A. Kogtenkova[1], N. S. Afonikova[1], O. K. Kamynina[1],
G. Faraji[2], M. Bulatov[3], D. Bradai[4]

†straumal@issp.ac.ru

[1]Osipyan Institute of Solid State Physics, Russian Academy of Sciences, Chernogolovka 142432, Russia
[2]School of Mechanical Engineering, College of Engineering, University of Tehran, Tehran 11155 – 4563, Iran
[3]Lomonosov Moscow State University, Moscow 119991, Russia
[4]Faculty of Physics, University of Sciences and Technology Houari Boumediene, Algiers 16111, Algeria

Abstract: During severe plastic deformation (SPD) of solid solutions, two processes occur simultaneously and compete with each other, namely the decomposition of a solid solution and dissolution of the second-phase precipitates. After a certain deformation, a steady-state concentration c_{ss} of the second component is reached in the solution during SPD. This concentration can be found at the solvus line in the phase diagram at the certain temperature T_{eff} (called usually effective temperature). The effect of high pressure torsion (HPT) on the structure of the Al-10 wt.% Mg alloy is studied. In a sample annealed at a temperature of 420°C, the HPT leads to a noticeable decomposition of the solid solution. In a sample annealed at a temperature of 300°C, a decrease in the concentration at HPT also occurs, but it is less than in the first case. Finally, in a sample annealed at a temperature of 200°C, there is practically no change in the concentration in the solid solution. This means that for Al-Mg alloys $c_{ss} = 3 \pm 0.3$ wt.% Mg. A comparison with the literature data for equal–channel angular pression (ECAP) of Al-Mg alloys gives approximately the same c_{ss} value for ECAP. This means that the effective temperature of T_{eff} in the Al-Mg alloys is close to 200°C.

Keywords: high pressure torsion, Al-Mg alloys, steady-state, solid solution, decomposition, precipitates, dissolution

Acknowledgements: *This research was funded by the Russian ministry of science and higher education (contract no. 075-15-2024-652 grant no. 13.2251.21.0252).*

1. Introduction

The idea of severe plastic deformation (SPD) goes back to the fundamental works of Bridgman [1]. Bridgman proposed methods when straining occurs without destroying the sample and practically without changing its external shape. The boom in SPD research began in the mid-nineties [2]. In particular, it was found that the SPD not only leads to exceptional grain refinement, but also allows the mechanical mixing of a wide variety of materials. It permits us to achieve a high non-equilibrium concentration of the dissolved component in a solid solution [3]. Formally, it is possible to reach by SPD the very high degrees of deformation. Nevertheless, the defects in the crystal lattice cannot accumulate indefinitely, but the process of their relaxation begins. As a result, the formation and annihilation of defects come to the dynamic equilibrium and a steady-state arises [4 – 8]. Thus, the grain size, mechanical properties, the particle size of the second phase, the composition of the solid solution etc. reach a steady-state value.

Initially, it seemed that if a material containing a mixture of different phases and components is subjected to SPD, then the components always mix. As a result, the atoms of the second component dissolve in the matrix and the solubility can reach a high non-equilibrium value. However, later the experimental facts began to appear that the opposite process can also take place. In other words, SPD can also cause the decomposition of a supersaturated solid solution [5]. A series of works was performed on copper-based binary alloys specially prepared from pure components [8]. It was found that during SPD, there is a competition between the formation and decomposition of a supersaturated solid solution. With increasing deformation, these two processes come to the dynamic equilibrium. As a result, a steady-state concentration c_{ss} of the second component in the solid solution is reached [4]. This steady-state concentration is equal to the solubility of the second component in the matrix at a certain temperature T_{eff} (it is usually called effective temperature). Usually, T_{eff} is higher than the temperature T_{SPD} of the SPD experiment. Most frequently, $T_{SPD} = 300$ K.

If a solid solution containing particles of the second phase is annealed at a temperature below T_{eff}, the concentration c in it will be lower than c_{ss}. Then, under SPD, the particles of

the second phase will dissolve and c will increase, striving to reach the c_{ss} value "from the left". If the sample is annealed at a temperature above T_{eff}, the concentration in the solid solution will be higher than c_{ss}. In this case, the solid solution will decompose during SPD, and the fine particles of the second phase will precipitate. As a result, the concentration in the solid solution will fall, trying to reach c_{ss} "from the right" [9]. In copper alloys, it was also found that the value of the steady-state concentration c_{ss} and, consequently, the effective temperature of T_{eff} depends both on the T_{SPD} [10] and on the activation enthalpy of the volume diffusion of the second component H_D. T_{eff} increases linearly with increasing H_D [9]. This is not surprising, since the jumps of atoms during mass transfer caused by SPD are associated with overcoming the same energy barrier as in conventional volume diffusion. As a result, the higher the energy barrier H_D, the more difficult diffusion relaxation occurs in SPD. Consequently, the steady-state c_{ss} concentration rises, as well as the effective temperature T_{eff}.

Thus, the competition between the formation and decomposition of a solid solution in SPD has been studied in detail for copper alloys. Unfortunately, there is currently only limited data on similar competition in aluminum-based alloys. Therefore, the goal of this work was to study the effect of high-pressure torsion (HPT) on the composition of a solid solution in Al-Mg alloys. The Al-Mg-based alloys that are very important for modern technologies. Therefore, many papers were published on the effects of various SPD methods on Al-Mg-based alloys. Between them are high pressure torsion [5,11–29], equal channel angular pressing (ECAP) [30–37], confined channel-die pressing (CCDP) [38], surface mechanical grinding treatment (SMGT) [39,40], friction stir processing (FSP) [41,42], accumulative roll bonding [43,44], different variants of extrusion [45–47], multi-directional forging (MDF) [48–50], rotary forging (swaging) [51,52], different variants of rolling [53–55], constrained groove pressing (CGP) [56,57], repetitive corrugation and straightening (RCS) [58], dynamic plastic deformation [59].

2. Materials and methods

The Al-10 wt.% Mg alloy was prepared from the high-purity 5N Al and 5N Mg using the vacuum induction melting. The ∅10 mm cylindrical Al-Mg ingots were cut using the spark erosion into 0.7 mm thick disks. Each disk was sealed into evacuated silica ampoule with a residual pressure of approximately 4×10^{-4} Pa. Samples were annealed at temperatures of 200°C for 1200 h, 300°C for 1200 h and 420°C for 500 h and then quenched in water. The 0.7 mm thick samples were subjected to HPT at room temperature, 5 revolutions of the plunger under pressure of 5 GPa at a rotation speed of 1 rpm, in a Bridgman anvil-type installation manufactured by W. Clement GmbH, Lang, Austria. After the HPT, the thickness of each sample was 0.35 mm. X-ray diffraction (XRD) patterns were obtained using Rigaku Smartlab X-ray diffractometer (Rigaku, Tokyo, Japan) under Cu-Kα1+α2 radiation, wavelength 0.15419 nm. Phase analysis and calculation of the lattice parameters were performed using the PowderCell 2.4 program. (PowderCell for Windows. Version 2.4. 08.03.2000, Werner Kraus and Gert Nolze, BAM, Berlin). The microstructure was also investigated using scanning electron microscopy (SEM). SEM characterization has been carried out using a Vega TS5130 MM (Tescan) microscope equipped with the LINK energy-dispersive spectrometer (Oxford Instruments).

3. Results and discussion

Figure 1 contains XRD patterns for Al-10 wt.% Mg alloy annealed at 420°C before (upper spectrum, red line) and after HPT (lower spectrum, black line). Figure 1b shows an enlarged peak (111), also before and after HPT. The XRD patterns contain only lines of the Al-based Al-Mg solid solution (denoted further as (Al)) with a face-centered cubic (FCC) lattice. The lines after HPT are noticeably widened compared to the lines in the annealed sample. This is due to a decrease in grain size under SPD. All peaks after HPT are shifted to the right compared to the peaks before HPT.

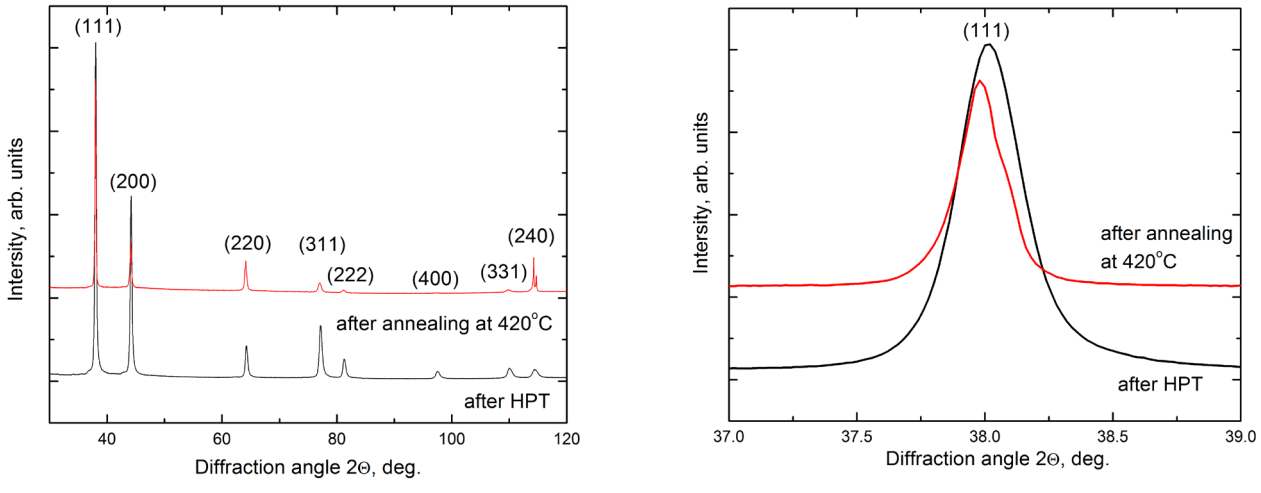

Fig. 1. (Color online) XRD patterns for Al-10 wt.% Mg alloy annealed at 420°C before (upper pattern, red line) and after HPT (lower pattern, black line). Figure 1b shows an enlarged (111) peak.

This means that the lattice period of the solid solution of the matrix decreases as a result of HPT.

Figure 2 shows the XRD patterns for the Al-10 wt.% Mg samples annealed at 200 and 300° C before (a) and after HPT (b). Black numbers indicate peaks from the FCC matrix (Al), and blue numbers indicate peaks from the Al_3Mg_2 phase. Peaks from the Al_3Mg_2 phase are present in all spectra both before and after HPT, however, they are significantly broadened after HPT. The peaks of the FCC phase (Al) are also broadened after HPT.

Figure 3 shows the values of the lattice period of a solid solution (Al) in samples annealed at different temperatures before (big red squares) and after HPT (small blue squares). The lattice period in the sample annealed at a temperature of 420°C decreases significantly after HPT. In a sample annealed at 300°C, the lattice period also decreases, but not as much as in the first sample. In a sample annealed at a temperature of 200°C, the lattice period of the matrix (Al) remains practically unchanged after HPT. The literature data for the ECAP of Al-7 wt.% Mg samples annealed at 500°C are also shown [32, 35, 36]. The lattice period in (Al) also decreases after ECAP. The decrease after 5 ECAP passes [32] is stronger than after 3 passes [35, 36]. Thick strokes on the right-hand side mark the lattice period in (Al) for 10 wt.% Mg (our sample annealed at 420°C), for 7 wt.% Mg (samples in Refs. [32, 35, 36] annealed at 500°C), and for our sample annealed at 200°C (point on the solvus line at about 3 wt.% Mg). These values were used to estimate the Mg content in (Al) for the phase diagram in Fig. 4.

Figure 4 shows an Al-rich part of the Al-Mg phase diagram. Solid black lines show the boundaries of the phase regions. The Mg concentration in the solid solution before and after HPT and ECAP was determined on the basis of XRD data on the lattice parameter (see Fig. 3). The red squares, as in Fig. 3, show the values of the Mg concentration in the (Al) solid solution after annealings. At 420°C and 500°C [32, 35, 36], the samples were in a single-phase (Al) region, so the Mg concentration in (Al) coincides with the total concentration of magnesium in the sample, 10 wt.% Mg and 7 wt.% Mg, respectively. At 200°C and 300°C, the Mg concentration in (Al) corresponds to a point on the solubility limit (solvus) line

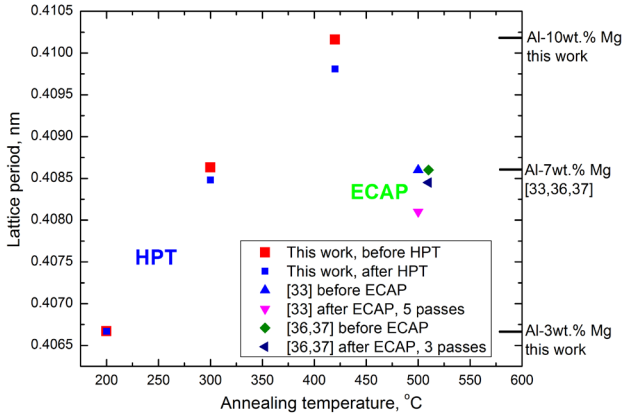

Fig. 3. (Color online) Lattice period of a solid solution (Al) in samples annealed at different temperatures before and after HPT, as well as before and after ECAP [32, 35, 36].

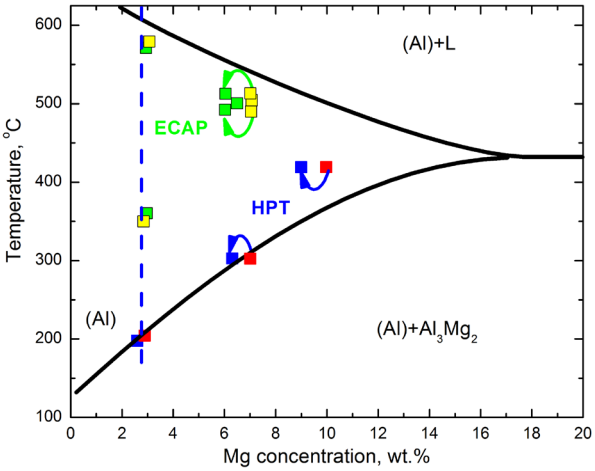

Fig. 4. (Color online) The Al-rich part of the Al-Mg phase diagram. Solid black lines show the boundaries of the phase regions (Al), (Al)+L and (Al)+Al_3Mg. The red and blue squares show the composition of the solid solution (Al) in the Al-10 wt.% Mg alloy samples, respectively, after annealing and after HPT. The vertical blue dotted line shows the concentration $c_{ss} = 3 \pm 0.3$ wt.% Mg. The yellow and green squares show the composition of the solid solution in the samples of alloys Al-7 wt.% Mg [32, 35, 36] and Al-3 wt.% Mg [31, 34] after annealing and after ECAP, respectively.

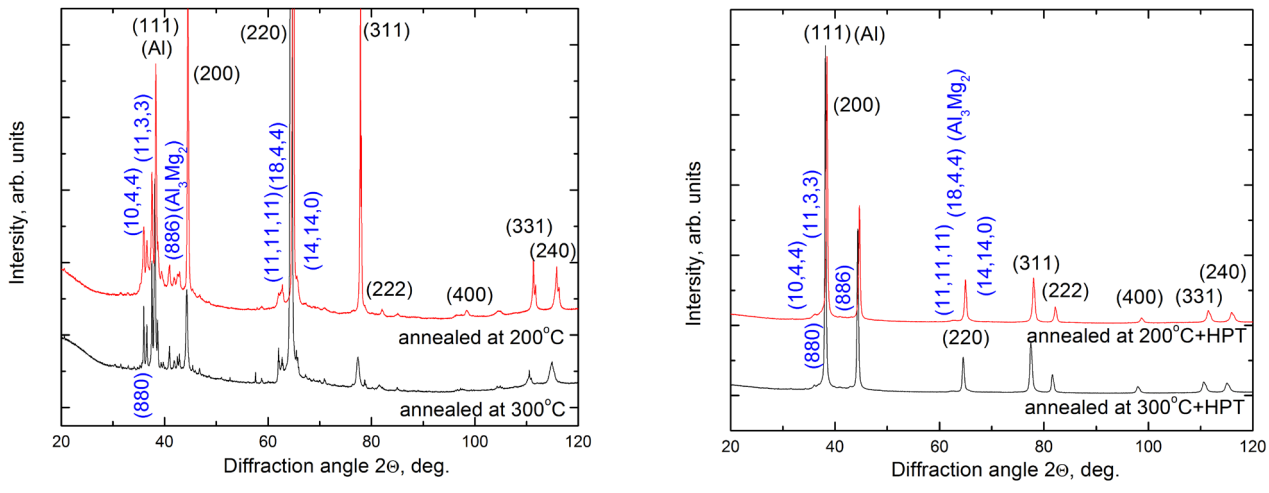

a b

Fig. 2. (Color online) XRD patterns for the Al-10 wt.% Mg samples annealed at 200 and 300°C before (a) and after (b) HPT.

of Mg in the (Al)-based solid solution. The blue squares show the composition of the solid solution in the Al-10 wt.% Mg alloy samples after HPT. The vertical blue dotted line shows the concentration value of $c_{ss} = 3 \pm 0.3$ wt.% Mg, to which the concentration in the solid solution tends after HPT. It can be interpreted as a steady-state concentration of c_{ss}, similar to that which we observed earlier after HPT of copper-based binary alloys [13]. However, differently to the Cu-Co as well as Cu-Ag and Cu-Sn alloys [13], the Mg content in the samples annealed at 420 and 300°C though moves towards c_{ss} after HPT, but does not reach it. Probably one needs for this purpose more than 5 anvil rotations.

The upper part of the figure shows the literature data for samples of alloys Al-7 wt.% Mg [32, 35, 36] and Al-3 wt.% Mg [31, 34] annealed at temperatures of 350 and 580°C, respectively (yellow squares), and then subjected to processing using ECAP (green squares). It is clearly seen that in samples with an initial magnesium concentration of 7 wt.% Mg, the ECAP treatment leads to a decrease in the lattice period [32, 35, 36], similar to how it happens with HPT. The shift after 5 ECAP passes [32] is stronger than after 3 passes [35, 36]. In samples with a magnesium content of 3 wt.% Mg [31, 34], the lattice period after ECAP remains almost unchanged, as in a sample with 3 wt.% Mg treated with HPT. This means that the steady-state concentration c_{ss} that occurs during SPD by the ECAP method coincides with the steady-state concentration c_{ss} that occurs during SPD by the HPT method.

It can be seen from Fig. 2 that in all three studied samples, the lattice period of the solid solution decreases during HPT. First of all, this may indicate the decomposition of a solid solution with the formation of particles of the second phase of Al_3Mg_2. It may be objected that Al_3Mg_2 lines do not appear on X-ray patterns after HPT in a single-phase sample pre-annealed at 420°C. It is known, however, that such particles formed during the decomposition of a solid solution are very small. Their size is no more than a dozen nanometers [7]. If there are few such particles, then additional lines do not appear in the X-ray patterns.

However, there is another possible reason for such a shift of X-ray diffraction lines after HPT in a single-phase sample pre-annealed at a 420°C. It is well known that with HPT, the grain size decreases significantly, and the specific GB area in the sample increases. If the second component segregates at GBs, then layers enriched with the second element should form at the new boundaries. Their formation requires atoms of the second component. If the samples have two-phases, then the GB enrichment can occur due to the partial dissolution of the particles of the second phase. If there is no second phase, and the sample consists only of a solid solution, then the segregation layers should form from the atoms dissolved in the volume. As a result, the concentration of the second component in the volume should decrease.

Thus, the displacement of XRD lines after HPT in a single-phase sample pre-annealed at a temperature of 420°C can be caused not only by the decomposition of the solid solution with the formation of very small Al_3Mg_2 particles, but also by the escape of magnesium atoms from the solid solution in volume to new GBs, which appear during HPT. In the samples annealed at temperatures of 200 and 300°C, the phase Al_3Mg_2 is already present before HPT. Therefore, the shift of X-ray peaks cannot be caused by the formation of GB segregation layers, but is associated only with the decomposition of the solid solution and the formation of new Al_3Mg_2 precipitates.

The GB enrichment in (Al) with magnesium atoms was predicted in theoretical calculations [60–62] and observed experimentally using atomic tomography [12,19,32]. However, the negative GB segregation was observed in aluminum-magnesium alloys in some GBs [12,18,39,63]. This means that the (Al)/(Al) GBs in these alloys can be not only enriched, but also depleted of magnesium. At such GBs, the concentration of magnesium is less than in volume. Thus, although the theory predicts only positive segregation, in real samples, magnesium segregation can be both positive and negative. The true ratio of GBs with positive and negative segregation in a polycrystal is unknown. If negative segregation prevails in the sample, then as a result of the formation of such boundaries during SPD, the solid solution in the volume should, on the contrary, be enriched rather than depleted.

4. Conclusions

1. High pressure torsion (HPT) of the Al-10 wt.% Mg annealed at different temperatures drives the decomposition of the (Al) solid solution.

2. The analysis of published data on equal channel angular pressing (ECAP) of Al-Mg alloys shows that ECAP also drives the decomposition of the (Al) solid solution.

3. If the Mg content in (Al) exceeds the value of 3 ± 0.3 wt.% Mg, this Mg concentration decreases both under HPT and ECAP.

4. In the samples with 3 ± 0.3 wt.% Mg HPT and ECAP do not change the Mg content in (Al).

5. Therefore, the value $c_{ss} = 3 \pm 0.3$ wt.% Mg was determined to be the steady-state Mg concentration in the (Al) solid solution for HPT and ECAP.

References

1. K. Edalati, Z. Horita, A review on high-pressure torsion (HPT) from 1935 to 1988, Mater. Sci. Eng. A 652 (2016) 325 – 352.
2. R. Z. Valiev, A. V. Koznikov, R. R. Mulyukov, Structure and properties of ultra-fine grained materials produced by severe plastic deformation, Mater. Sci. Eng. A 168 (1993) 141–148.
3. K. Kaneko, T. Hata, T. Tokunaga, Z. Horita, Fabrication and characterization of supersaturated Al-Mg alloys by severe plastic deformation and their mechanical properties, Mater. Trans. 50 (2009) 76 – 81.
4. B. B. Straumal, A. R. Kilmametov, Yu. Ivanisenko, A. A. Mazilkin, O. A. Kogtenkova, L. Kurmanaeva, A. Korneva, P. Zięba, B. Baretzky, Phase transitions induced by severe plastic deformation: steady-state and equifinality, Int. J. Mater. Res. 106 (2015) 657 – 664.
5. B. B. Straumal, B. Baretzky, A. A. Mazilkin, F. Phillipp, O. A. Kogtenkova, M. N. Volkov, R. Z. Valiev, Formation of nanograined structure and decomposition of supersaturated solid solution during high pressure torsion of Al-Zn and Al-Mg, Acta Mater. 52 (2004) 4469 – 4478.

6. B. B. Straumal, R. Kulagin, L. Klinger, E. Rabkin, P. B. Straumal, O. A. Kogtenkova, B. Baretzky, Structure refinement and fragmentation of precipitates under severe plastic deformation: A review, Materials 15 (2022) 601.
7. B. B. Straumal, S. G. Protasova, A. A. Mazilkin, E. Rabkin, D. Goll, G. Schütz, B. Baretzky, R. Valiev, Deformation-driven formation of equilibrium phases in the Cu-Ni alloys, J. Mater. Sci. 47 (2012) 360 – 367.
8. B. B. Straumal, A. R. Kilmametov, A. Korneva, A. A. Mazilkin, P. B. Straumal, P. Zięba, B. Baretzky, Phase transitions in Cu-based alloys under high pressure torsion, J. Alloys Comp. 707 (2017) 20 – 26.
9. B. B. Straumal, A. R. Kilmametov, B. Baretzky, O. A. Kogtenkova, P. B. Straumal, L. Lityńska-Dobrzyńska, R. Chulist, A. Korneva, P. Zięba, High pressure torsion of Cu-Ag and Cu-Sn alloys: limits for solubility and dissolution, Acta Mater. 195 (2020) 184 –198.
10. B. B. Straumal, A. R. Kilmametov, P. B. Straumal, A. A. Mazilkin, Decrease of steady-state solubility of Ag in Cu by high-pressure torsion at low temperature, J. Mater. Sci. 59 (2024) 5818 – 5830.
11. D. C. Machado, P. Cibely, A. Flausino, Y. Huang, P. R. Cetlin, T. G. Langdon, P. H. R. Pereira, Influence of processing temperature on microhardness evolution, microstructure and superplastic behaviour in an Al-Mg alloy processed by high-pressure torsion, J. Mater, Res. Technol. 24 (2023) 2850 – 2867.
12. J. Xue, S. Jin, X. Anb, X. Liao, J. Li, G. Sha, Understanding formation of Mg-depletion zones in Al-Mg alloys under high pressure torsion, J. Mater. Sci. Technol. 35 (2019) 858 – 864.
13. J.-K. Han, J. Jang, T. G. Langdon, M. Kawasaki, Bulk-state reactions and improving the mechanical properties of metals through high-pressure torsion, Mater. Trans. 60 (2019) 1131–1138.
14. M. Kawasaki, J.-K. Han, D.-H. Lee, J. Jang, T. G. Langdon, Fabrication of nanocomposites through diffusion bonding under high-pressure torsion, J. Mater. Res. 33 (2018) 2700 – 2710.
15. Y. Tang, W. Goto, S. Hirosawa, Z. Horita, S. Lee, K. Matsuda, D. Terada, Concurrent strengthening of ultrafine-grained age-hardenable Al-Mg alloy by means of high-pressure torsion and spinodal decomposition, Acta Mater. 131 (2017) 57 – 64.
16. M. Kawasaki, T. G. Langdon, Using severe plastic deformation to fabricate strong metal matrix composites, Mater. Res. 20 (2017) 46 – 52.
17. K. Edalati, D. Akama, A. Nishio, S. Lee, Y. Yonenaga, J. M. Cubero-Sesin, Z. Horita, Influence of dislocation-solute atom interactions and stacking fault energy on grain size of single-phase alloys after severe plastic deformation using high-pressure torsion, Acta Mater. 69 (2014) 68 – 77.
18. X. Sauvage, A. Ganeev, Y. Ivanisenko, N. Enikeev, M. Murashkin, R. Valiev, Grain boundary segregation in UFG alloys processed by severe plastic deformation, Adv. Eng. Mater. 14 (2012) 968 – 974.
19. R. Z. Valiev, N. A. Enikeev, M. Yu. Murashkin, V. U. Kazykhanova, X. Sauvage, On the origin of the extremely high strength of ultrafine-grained Al alloys produced by severe plastic deformation, Scripta Mater. 63 (2010) 949 – 952.
20. M. Liu, H. J. Roven, X. Liu, M. Murashkin, R. Z. Valiev, T. Ungár, L. Balogh, Grain refinement in nanostructured Al-Mg alloys subjected to high pressure torsion, J. Mater. Sci. 45 (2010) 4659 – 4664.
21. M. Liu, H. J. Roven, X. Liu, M. Murashkin, R. Z. Valiev, T. Ungár, L. Balogh, Special nanostructures in Al-Mg alloys subjected to high pressure torsion, Trans. Nonferr. Met. Soc. China 20 (2010) 2051– 2056.
22. M. Liu, H. J. Roven, X. Liu, M. Murashkin, R. Z. Valiev, Structural characterization by high-resolution electron microscopy of an Al-Mg alloy processed by high-pressure torsion, Mater. Sci. Eng. A 503 (2009) 122 –125.
23. A. A. Mazilkin, B. B. Straumal, S. G. Protasova, O. A. Kogtenkova, R. Z. Valiev, Structural changes in Al alloys upon the severe plastic deformation, Phys. Sol. State 49 (2007) 868 – 873.
24. A. A. Mazilkin, B. B. Straumal, E. Rabkin, B. Baretzky, S. Enders, S. G. Protasova, O. A. Kogtenkova, R. Z. Valiev, Softening of nanostructured Al-Zn and Al-Mg alloys after severe plastic deformation, Acta Mater. 54 (2006) 3933 – 3939.
25. A. A. Mazilkin, B. Baretzky, S. Enders, O. A. Kogtenkova, B. B. Straumal, E. I. Rabkin, R. Z. Valiev, Hardness of nanostructured Al-Zn, Al-Mg and Al-Zn-Mg alloys obtained by high-pressure torsion, Def. Diff. Forum 249 (2006) 155 –160.
26. M. Liu, S. Sun, H. J. Roven, Y. Yu, Z. Zhang, M. Murashkin, R. Z. Valiev, Deformation defects and electron irradiation effect in nanostructured Al-Mg alloy processed by severe plastic deformation, Trans. Nonferr. Met. Soc. China 22 (2012) 1810 –1816.
27. P. Bazarnik, B. Romelczyk, Y. Huang, M. Lewandowska, T. G. Langdon, Effect of applied pressure on microstructure development and homogeneity in an aluminium alloy processed by high-pressure torsion, J. Alloys Compd. 688 (2016) 736 – 745.
28. X. Sauvage, N. Enikeev, R. Valiev, Y. Nasedkina, M. Murashkin, Atomic-scale analysis of the segregation and precipitation mechanisms in a severely deformed Al-Mg alloy, Acta Mater. 72 (2014) 125 –136.
29. W. Xu, Y. C. Xin, B. Zhang, X. Y. Li, Stress corrosion cracking resistant nanostructured Al-Mg alloy with low angle grain boundaries, Acta Mater. 225 (2022) 117607.
30. Z. Horita, D. J. Smith, M. Furukawa, M. Nemoto, R. Z. Valiev, T. G. Langdon, An investigation of grain boundaries in submicrometer-grained Al-Mg solid solution alloys using high-resolution electron microscopy, J. Mater. Res. 11 (1996) 1880 –1890.
31. T. Morishige, Y. Suzuki, T. Aizawa, T. Tanaka, T. Hirata, T. Takenaka, Microstructural evolution and distributions of grain boundary in SPD processed Al-3 mass%Mg alloy, Mater. Trans. 64 (2023) 983 – 987.
32. M. Zha, H.-M. Zhang, X.-T. Meng, H.-L. Jia, S.-B. Jin, G. Sha, H.-Y. Wang, Y.-J. Li, H. J. Roven, Stabilizing a severely deformed Al-7Mg alloy with a multimodal grain structure via Mg solute segregation, J. Mater. Sci. Technol. 89 (2021) 141–149.
33. R. Kalsar, D. Yadav, A. Sharma, H.-G. Brokmeier, J. May, H. W. Höppel, W. Skrotzki, S. Suwas, Effect of Mg content on microstructure, texture and strength of severely equal

channel angular pressed aluminium-magnesium alloys, Mater. Sci. Eng. A 797 (2020) 140088.
34. T. Tański, P. Snopiński, K. Prusik, M. Sroka, The effects of room temperature ECAP and subsequent aging on the structure and properties of the Al-3%Mg aluminium alloy, Mater. Charact. 133 (2017) 185–195.
35. M. Zha, Y. Li, R. H. Mathiesen, R. Bjørge, H. J. Roven, High ductility bulk nanostructured Al-Mg binary alloy processed by equal channel angular pressing and inter-pass annealing, Scripta Mater. 105 (2015) 22 – 25.
36. M. Zha, Y. Li, R. H. Mathiesen, R. Bjørge, H. J. Roven, Microstructure evolution and mechanical behavior of a binary Al-7Mg alloy processed by equal-channel angular pressing, Acta Mater. 84 (2015) 42 – 54.
37. M. Yu. Murashkin, I. Sabirov, V. U. Kazykhanov, E. V. Bobruk, A. A. Dubravina, R. Z. Valiev, Enhanced mechanical properties and electrical conductivity in ultrafine-grained Al alloy processed via ECAP-PC, J. Mater. Sci. 48 (2013) 4501 – 4509.
38. S. Zhao, C. Meng, F. Mao, W. Hu, G. Gottstein, Influence of severe plastic deformation on dynamic strain aging of ultrafine grained Al-Mg alloys, Acta Mater. 76 (2014) 54 – 67.
39. W. Xu, B. Zhang, K. Du, X. Y. Li, K. Lu, Thermally stable nanostructured Al-Mg alloy with relaxed grain boundaries, Acta Mater. 226 (2022) 117640.
40. Q. Sun, X. Guo, F. Cao, Surface mechanical treatment suppressing the strength-corrosion trade-off in an Al-Mg binary alloy, Surf. Coat. Technol. 444 (2022) 128654.
41. J. Xie, L. Mei, X. Chen, Y. Cao, W. Lu, G. Huang, Strength-ductility synergy via cryogenic severe plastic deformation in an Al-Mg alloy, achieved by clustering-induced strengthening, Mater. Res. Lett. 12 (2024) 373 – 380.
42. F. Khodabakhshi, A. P. Gerlich, On the correlation between indentation hardness and tensile strength in friction stir processed materials, Mater. Sci. Eng. A 789 (2020) 139682.
43. I. Bencherifa, B. Alili, T. Baudin, F. Brisset, D. Thiaudière, C. Mocuta, D. Bradai, On the microstructure and texture of intermetallics in Al/Mg/Al multi-layer composite fabricated by Accumulative Roll Bonding. Micron 173 (2023) 103507.
44. Z. Sarvi, A. Sadeghi, M. M. Mashhadi, Stoichiometry and texture evolution of individual layers during accumulative roll bonding of Al-Mg laminated composites, JMEPEG 32 (2023) 8358 – 8366.
45. T. Tian, M. Zha, H.-L. Jia, Z.-M. Hua, P.-K. Ma, H.-Y. Wang, The effect of high solid solution Mg contents (7 – 13wt.%) on the dynamic strain aging behavior of Al-Mg alloys, Mater. Sci. Eng. A 880 (2023) 145376.
46. R. Goswami, P. S. Pao, S. B. Qadri, R. L. Holtz, Severe plastic deformation induced sensitization of cryo-milled nanocrystalline Al-7.5 Mg, Metal. Mater. Trans. A 45 (2014) 2894 – 2898.
47. J. Hu, W. Zhang, D. Fu, J. Teng, H. Zhang, Improvement of the mechanical properties of Al-Mg-Si alloys with nano-scale precipitates after repetitive continuous extrusion forming and T8 tempering, J. Mater. Res/Technol. 8 (2019) 5950 – 5960.
48. O. Sh. Sitdikov, E. V. Avtokratova, B. I. Atanov, M. V. Markushev, Effect of multidirectional isothermal forging on the formation of ultrafine-grained structure in alloy 1570C, Inorg. Mater. 58 (2022) 544 – 554.
49. A. V. Mikhaylovskaya, A. D. Kotov, M. S. Kishchik, A. S. Prosviryakov, V. K. Portnoy, The effect of isothermal multi-directional forging on the grain structure, superplasticity, and mechanical properties of the conventional Al-Mg-based alloy, Metals 9 (2019) 33.
50. A. Neetu, S. Singh, P. N. Rao, R. Jayaganathan, A. Midathada, K. Verma, U. K. Ravella, Elevated corrosion in strain hardened Al-Mg alloy, Vacuum 157 (2018) 402 – 413.
51. S. O. Rogachev, V. A. Andreev, V. S. Yusupov, S. A. Bondareva, V. M. Khatkevich, E. V. Nikolaev, Effect of rotary forging on microstructure evolution and mechanical properties of aluminum alloy/copper bimetallic material, Met. Mater. Int. 28 (2022) 1038 – 1046.
52. M. Abdulstaar, M. Mhaede, M. Wollmann, L. Wagner, Investigating the effects of bulk and surface severe plastic deformation on the fatigue, corrosion behaviour and corrosion fatigue of AA5083, Surf. Coat. Technol. 254 (2014) 244 – 251.
53. M. Y. Amegadzie, D. P. Bishop, Effect of asymmetric rolling on the microstructure and mechanical properties of wrought 6061 aluminum. Mater. Today Comm. 25 (2020) 101283.
54. P. Kumar, A. Singh, Investigation of fracture behaviour and low cycle fatigue properties of cryorolled Al-Mg alloy, Theor. Appl. Fract. Mech. 98 (2018) 78 – 94.
55. D. H. Jang, Y. B. Park, W. J. Kima, Significant strengthening in superlight Al-Mg alloy with an exceptionally large amount of Mg (13 wt%) after cold rolling, Mater. Sci. Eng. A 744 (2019) 36 – 44.
56. M. Moradpour, F. Khodabakhshi, H. Eskandari, Dynamic strain aging behavior of an ultra-fine grained Al-Mg alloy (AA5052) processed via classical constrained groove pressing, J. Mater. Res. Techhol. 8 (2019) 630 – 643.
57. J. Mozafari, F. Khodabakhshi, H. Eskandari, M. Haghshenas, Wear resistance and tribological features of ultra-fine-grained Al-Mg alloys processed by constrained groove pressing-cross route, JMEPEG 28 (2019) 1235 – 1252.
58. N. Thangapandian, S. Balasivanandha Prabu, K. A. Padmanabhan, Effects of die profile on grain refinement in Al-Mg alloy processed by repetitive corrugation and straightening, Mater. Sci. Eng. A 649 (2016) 229 – 238.
59. S. Jin, N. Tao, K. Marthinsen, Y. Li, Deformation of an Al-7Mg alloy with extensive structural micro-segregations during dynamic plastic deformation, Mater. Sci. Eng. A 628 (2015) 160 – 167.
60. V. I. Razumovskiy, A. V. Ruban, I. M. Razumovskii, A. Y. Lozovoi, V. N. Butrim, Y. K. Vekilov, The effect of alloying elements on grain boundary and bulk cohesion in aluminum alloys: An ab initio study, Scr. Mater. 65 (2011) 926 – 929.
61. H. Wang, M. Kohyama, S. Tanaka, Y. Shiihara, First-principles study of Si and Mg segregation in grain boundaries in Al and Cu: application of local-energy decomposition, J. Mater. Sci. 50 (2015) 6864 – 6881.
62. X.-Y. Liu, J. B. Adams, Grain-boundary segregation in Al-10%Mg alloys at hot working temperatures, Acta Mater. 46 (1998) 3467 – 3476.
63. D. C. Paine, G. C. Weatherly, K. T. Aust, A STEM study of grain-boundary segregation in Al-6.5 wt% Mg alloy, J. Mater. Sci. 21 (1986) 4257 – 4261.